Eur. Phys. J. E (2019) **42**: 91
DOI 10.1140/epje/i2019-11855-2

THE EUROPEAN PHYSICAL JOURNAL E

Regular Article

Friction weakening by mechanical vibrations: A velocity-controlled process

V. Vidal[1], C. Oliver[2], H. Lastakowski[1], G. Varas[2], and J.-C. Géminard[1,a]

[1] Université de Lyon, Laboratoire de Physique, ENS de Lyon, CNRS, F-69342 Lyon, France
[2] Instituto de Fisica, Pontificia Universidad Católica de Valparaiso, Av. Universidad 330, Valparaiso, Chile

Received 21 March 2019 and Received in final form 10 June 2019
Published online: 18 July 2019

Abstract. Frictional weakening by vibrations was first invoked in the 70s to explain unusual fault slips and earthquakes, low viscosity during the collapse of impact craters or the extraordinary mobility of sturzstroms, peculiar rock avalanches which travels large horizontal distances. This mechanism was further invoked to explain the remote triggering of earthquakes or the abnormally large runout of landslides or pyroclastic flows. Recent experimental and theoretical works pointed out that the key parameter which governs frictional weakening in sheared granular media is the characteristic velocity of the vibrations. Here we show that the mobility of the grains is not mandatory and that the vibration velocity governs the weakening of both granular and solid friction. The critical velocity leading to the transition from stick-slip motion to continuous sliding is in both cases of the same order of magnitude, namely a hundred microns per second. It is linked to the roughness of the surfaces in contact.

1 Introduction

"It is easier to further the motion of a moving body than to move a body at rest." This sentence written by Themistius (about A.D. 320–390) is the first record of friction in history [1]. Since then, the frictional motion of a single body over a fixed substrate or of a sheared granular assembly revealed a wide variety of behaviors. At low shear velocity, the system experiences a stick-slip motion, with the alternance of energy loading phases (system at rest) and quick energy release phases (sudden slip). Upon increase of the shear velocity, a transition to continuous sliding is reported [2–5]. During catastrophic events such as earthquakes, landslides or pyroclastic flows, puzzling phenomena of frictional weakening were reported: friction decreases with the shear velocity [6–9]. Melosh [10] first proposed in 1979 that vibrations due to pressure fluctuations and the resulting strain release could temporarily reduce the normal stress, and thus decrease the shear-stress threshold to trigger sliding motion [11]. This mechanism, initially called *vibrational fluidization*, and later *acoustic fluidization* [10,11], was further thought to be at the origin of dramatic events, such as earthquakes, remotely triggered by external waves [12,8].

How does endogenous noise or external mechanical disturbances drastically affect the frictional properties? In the last decades, many works have attempted to tackle this issue. They have shown that vibrations reduce or even suppress friction [13–22]. Interpretations were proposed based on a non-monotonic flow curve, leading to instabilities and self-fluidization [23,24], softening effect due to non-linearity at the grains contact [25], contact opening [26,27] or sliding [28]. In models considering the sliding of a single solid block, the acceleration characterizing the vibration has often been stated as the parameter governing the transition between stick-slip motion and continuous sliding, with a threshold equal to the gravitational acceleration [19]. However, Lastakowski *et al.* pointed out recently that the *velocity* characterizing the vibration, and not the acceleration, is the parameter governing the frictional weakening in granular assemblies [21]. Surprisingly, the sheared granular material exhibits a transition between stick-slip motion and continuous sliding for very low values of the vibration velocity, around $100\,\mu$m/s, independently of most parameters which can be varied in the system (driving velocity, grain size and material, granular layer thickness, ...). This result is independent of the average velocity of the solid, contrary to what is expected from the classical rate-and-state heuristic models [29,30, 3,5]. A recent microscopic model based on sliding contacts under vibrations in a granular assembly successfully explains the dependence of the transition on the vibration velocity [28]. However, important questions arise: Is the grains mobility mandatory for the system to exhibit

[a] e-mail: jean-christophe.geminard@ens-lyon.fr

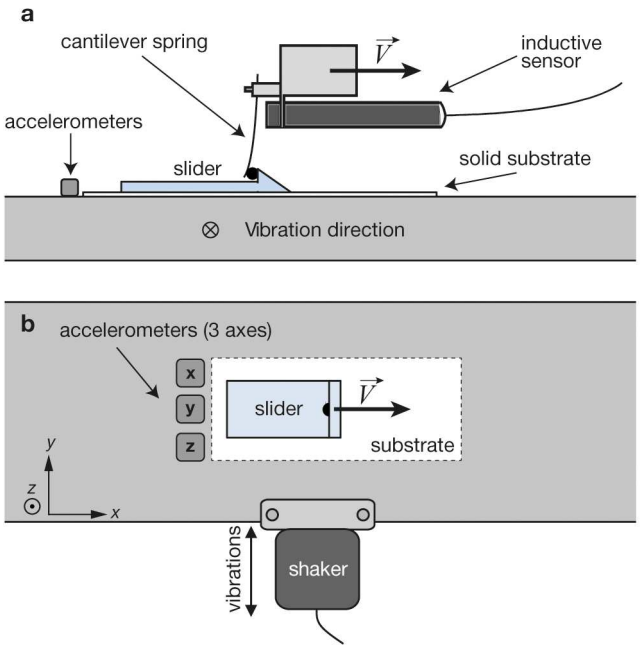

Fig. 1. Sketch of the experimental setup. (a) Side view. (b) Top view. Different substrates are used in the experiment. In the case of granular materials, the accelerometers are located at the bottom of the granular layer, aligned with the shaker.

this transition? Does the velocity characterizing the vibration remain the parameter governing the transition in solid friction too? Here we address these questions by studying experimentally solid (paper-paper) friction in the presence of harmonic vibrations.

2 Experimental setup

The setup (fig. 1) is similar to the one used by Lastakowski *et al.* to further compare the frictional weakening under vibrations in both solid and granular friction in the same experimental configuration [21]. The slider, made of plexiglass, of length 9 cm and width 6 cm, is pulled across a fixed substrate by means of a cantilever spring (metallic blade of stiffness k). A steel ball is glued at the front of the slider to ensure a punctual contact so that no significant torque is applied to the slider. The blade is mounted on a translational stage (Schnaefler Technologies Sechnr) driven at constant velocity V: A DC motor (Crouzet, 5 N.m, 17 W) coupled with different reduction gears (Crouzet 1.04, 10, 100 RPM) sets velocities between 18 and 7700 μm/s. An inductive sensor (Baumer, IPRM 12I9505/S14) measures the blade deflection at a rate of 2 kHz. From the variations of the blade deflection in time, we derive the instantaneous shear force F applied to the slider, and denote $F^* = F/mg$ the dimensionless force, where $m \simeq (22 \pm 5)$ g is the slider mass and $g = 9.8\,\mathrm{m \cdot s^{-2}}$ the gravitational acceleration.

Paper-paper friction is investigated by using two types of paper: smooth printer paper (Inapa tecno copy-/laser pro laser, 80 g/m^2, white) and rough drawing paper (Canson®, Papier dessin blanc C grain, 180 g/m^2). To ensure reproducible experiments, both the surface below the slider and upon the substrate are prepared according to the following protocol: first, the samples are cut carefully, without touching the surface to avoid contamination and modification of its properties; a first sheet of large dimensions (length 21 cm, width 9 cm) is stuck on the solid substrate; a second sheet cut at the slider's dimensions is stuck below the slider, ensuring a paper-paper frictional contact (fig. 1). For each given set of parameters (driving velocity V, spring stiffness k, vibrations amplitude and frequency), three runs are performed with the same paper samples to check the reproducibility. The samples are then removed from both the substrate and the slider bottom face and replaced by new ones, to avoid damage and sample aging due to repetitive friction of the surfaces. The first experiment with the new samples is made with the previous set of parameters, to test reproducibility from one sample to the other, then parameters are changed, three runs are performed, and so on. To avoid variations due to atmospheric conditions, the experiment is placed as a whole inside a large box of controlled temperature T and humidity R_H. For all experiments on paper-paper friction, $T = (35 \pm 2)$°C and $R_H = (20 \pm 2)$%. Results for granular material are inferred from the analysis of the previous experimental data of Lastakowski *et al.* [21].

Vibrations are imposed to the entire experimental setup by a shaker (Brüel & Kjær, type 4810 + amplifier 2706) clamped on the substrate (a duralumin plate). It applies horizontal harmonic vibrations along the y-axis, perpendicular to the driving direction (fig. 1). The vibrations amplitude A and frequency ω are measured *in situ* close to the slider, at the surface of the solid substrate, by three accelerometers (Dytran Instrument, model # 3035BG) giving the three components of the acceleration. Before performing any experiment, we check that the local acceleration is correctly oriented in the y-direction, and constant over a region large enough to include the slider path. We avoid resonances of any part of the experimental setup. Note that for the experiments on granular friction, the local acceleration was measured by sticking the accelerometers at the bottom of the granular layer, below the slider trajectory.

Additional SEM and AFM measurements were performed to investigate the link between the weakening of the frictional properties and the roughness of the surfaces in frctional contact. Scanning Electron Microscopy (SEM) images were adquired on a Supra 55, VP Zeiss. Atomic Force Microscopy (AFM) measurements were performed on a commercial apparatus (NanoWizard® 4 AFM, JPK Instruments) on paper samples at different spatial resolution (256×256 pixels for a spatial extent ranging from 0.352×0.352 to $100 \times 100\,\mu$m).

3 Weakening of granular or solid friction

The driving velocity V, slider mass m and spring stiffness k are chosen such that, in absence of vibrations,

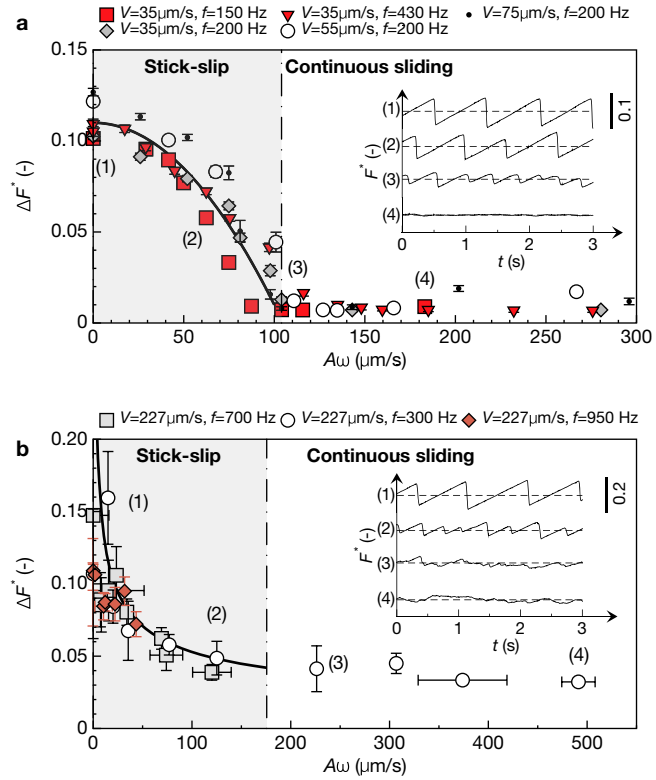

Fig. 2. Normalized force applied on the slider, F^* for (a) granular and (b) solid (paper-paper, Inapa) friction (black lines are guides to the eye). Insets: examples of normalized force as a function of time when increasing the vibration velocity, $(A\omega)$, for (a) granular ($k = 870\,\mathrm{N/m}$, $V = 35\,\mu\mathrm{m/s}$, red squares in (a)) and (b) solid friction ($k = 170\,\mathrm{N/m}$, $V = 227\,\mu\mathrm{m/s}$, white circles in (b)). Note that for large $(A\omega)$ in solid friction, the stick-slip amplitude decreases but never vanishes, although in (4), the slider does not experience any more stick-slip motion but rather a continuous sliding with force fluctuations (the dashed line represents the average of the signal, and the vertical line is the scalebar for all the data).

the slider continuously experiences a well-defined stick-slip motion, characterized by a sawtooth shape of the instantaneous force applied to the slider as a function of time (upper signal, insets figs. 2(a), (b)). At given vibration frequency $f = \omega/2\pi$, upon increase of the vibration amplitude, the amplitude, ΔF^*, of the force signal decreases (insets figs. 2(a), (b)).

For granular friction, previous results pointed out that the vibration velocity, $(A\omega)$, is the parameter governing frictional weakening. Reanalyzing the data from Lastakowski *et al.* [21], we evidence this dependence showing that the amplitude ΔF^* is a function of the velocity $A\omega$, independent of the frequency ω (fig. 2(a)). Note also that ΔF^* does not depend on the driving velocity V (as long as it is small enough for the system to be in the stick-slip regime in absence of vibration). Finally, the well-marked transition, at a critical vibration velocity $(A\omega)_c \sim 100\,\mu\mathrm{m/s}$, is found independent of most experimental parameters (grain shape and material, driving velocity, granular layer thickness, etc.) [21].

For solid friction, we now report a weakening and, also, a transition to continuous sliding upon increase of the vibration amplitude (fig. 2(b)). The vibration velocity, $(A\omega)$, is again the governing parameter for the decay of the stick-slip amplitude, ΔF^*, independently of the driving velocity V. Interestingly, some differences appear between solid and granular friction. For Inapa paper, the shape of the frictional weakening is concave, and does not display any clear transition between stick-slip and continuous sliding as in granular assemblies. The gray zone, which indicates the region where stick-slip motion occurs, is delimitated by checking the force signals (fig. 2(b), inset) and picking the vibration velocity above which the slider spends less than half the time in the rest phase, marked by linear increases in the force signal. The critical velocity for Inapa paper, $(A\omega)_c = (170 \pm 50)\,\mu\mathrm{m/s}$, even if larger, remains of the same order of magnitude than for granular friction.

4 Role of roughness in frictional weakening

First, we can wonder if the critical vibration velocity is enough, by simple addition to the imposed driving velocity, to overcome the driving velocity necessary to undergo the transition between stick-slip and continuous sliding in absence of vibrations. Figure 3(a) (top) displays the normalized force exerted on the slider as a function of time for different driving velocity V in absence of vibration, *e.g.* $(A\omega) = 0$. We observe that the continuous steady sliding regime, which requires large driving velocity V, is never reached in the experimental range (up to 7 mm/s). In addition, we observe a transition between stick-slip motion and the inertial regime [5] for a velocity of the order of 5 mm/s, much larger than $(A\omega)_c$. The typical driving velocity V leading to the transition in absence of vibration is thus at least one order of magnitude larger than the velocity associated with the vibrations responsible for the transition to continuous sliding. Therefore, a simple velocity composition has to be discarded to explain the transition to continuous sliding when vibrations are imposed.

Second, since the pioneering work of Bowden and Tabor [31], it is known that roughness plays a major role in friction. To test its influence on frictional weakening by vibrations, we performed additional experiments on Canson®, a commercial paper which exhibits a rough surface traditionally used for charcoal drawing. As for Inapa paper, the driving velocity alone is never enough, in our experimental range, to provoke the transition between stick-slip motion and continuous sliding (fig. 3(a), bottom). In the presence of vibrations, frictional weakening is observed. Once again, all data collapse when displaying the amplitude, ΔF^*, of the force variations as a function of the vibration velocity, $(A\omega)$ (fig. 3(b), red line). Note that similarly to granular assemblies, the shape of the frictional weakening curves for solid friction is robust for different spring constant k and driving velocity V (fig. 3(b)). Changing the paper surface properties induces a change

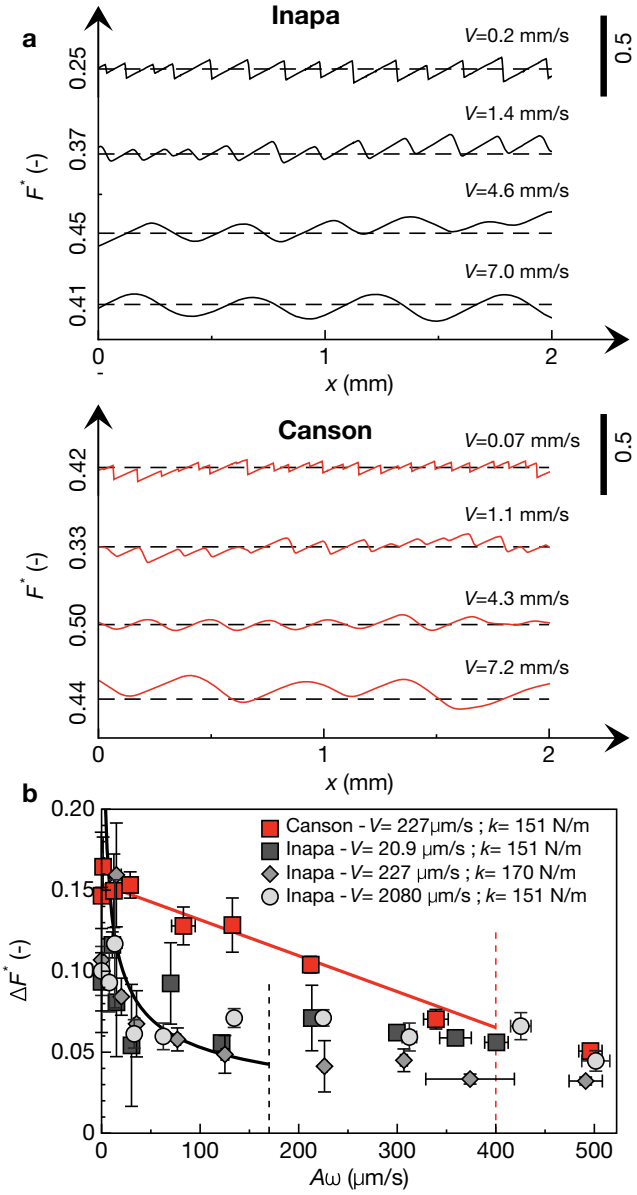

Fig. 3. Solid (paper-paper) friction dependence on driving velocity V or vibration velocity $(A\omega)$. (a) Normalized force F^* as a function of time t for different driving velocities V, in absence of vibration (top: Inapa paper; bottom: Canson® paper; $k = 170\,\mathrm{N/m}$). The average value $\langle F^* \rangle$ of the dimensionless force F^* (dashed lines) depends not only on the driving velocity V but also on the location of the slider on the substrate (due to the heterogeneity of the surfaces in frictional contact). This explains the apparent non-monotonic behavior of $\langle F^* \rangle$ *vs.* V. (b) Amplitude ΔF^* of the normalized force variations for Inapa (gray and black) and Canson® (red) paper as a function of the vibration velocity, $(A\omega)$ (solid lines are guide to the eye, $f = 300\,\mathrm{Hz}$).

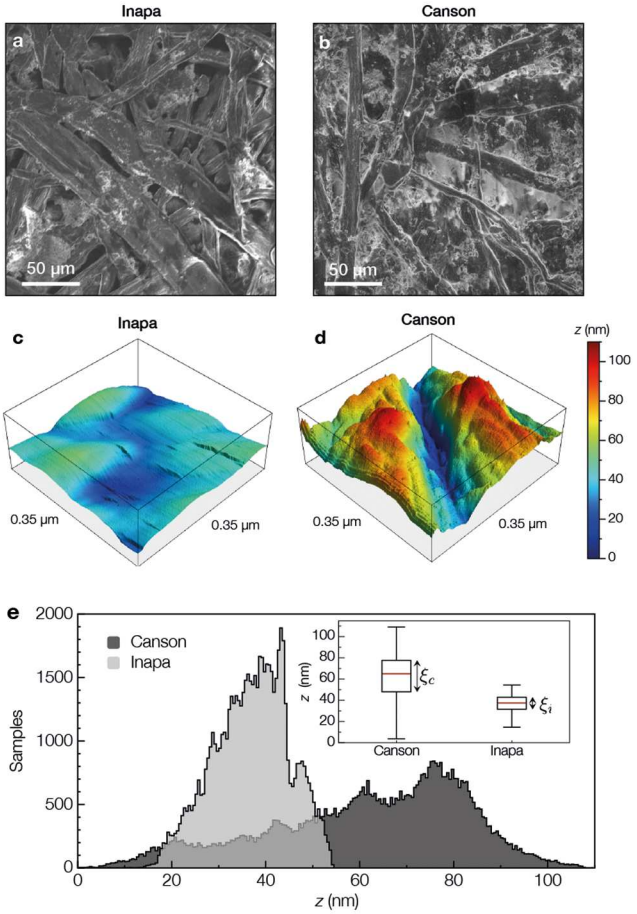

Fig. 4. Surface roughness analysis. (a), (b): SEM images of Canson® (a) and Inapa (b) papers (Supra 55, VP Zeiss). Note that the fibers are larger for Inapa paper, although the paper surface is smoother. (c), (d): AFM topographic map of $0.35\,\mu\mathrm{m} \times 0.35\,\mu\mathrm{m}$ samples of Canson® (a) and Inapa (b) papers (NanoWizard® 4, JPK Instruments). The colorbar indicates the height in nanometers. (e) Height distribution. Inset: box plot representation. The box size represents the IQR (InterQuartile Range) and gives an estimation of the typical height ξ of the asperities.

not only in the curve shape, which exhibits a linear decrease for Canson®, but also on the critical vibration velocity, here $(A\omega)_c \simeq 400\,\mu\mathrm{m/s}$ (vertical red dashed line, fig. 3(b)).

To further investigate the link between frictional weakening and surface properties, it is necessary to characterize the roughness. However, quantifying the typical scale of asperities is not straightforward, as materials can display multiscale roughness distributions. It is the case for paper, a complex entangled fibers network [32]. The typical size of the fibers is clearly not the relevant scale, as they are most probably flattened during paper manufacturing. Indeed, Canson® has a rougher surface, although its fibers are thinner than those of Inapa paper (fig. 4(a), (b)). The nanometer range has ultimately been acknowledged as the most relevant spatial scale for contacts [5]. AFM measurements on both paper samples show that the topography at small scale is clearly different, with rough linear structures for Canson® (fig. 4(d)) in contrast to smoother bumps for Inapa (fig. 4(c)). The typical scale of the asperities, ξ, is estimated from the topography distribution (fig. 4(e))

Table 1. Characterization of the asperities: typical height ξ obtained with IQR (see fig. 4(e)), typical vertical (l_R) and horizontal (w) lengths, aspect ratio l_R/l_w and radius of curvature R. Average values for glass beads are taken from [33].

	Canson®	Inapa	Glass beads
ξ (nm)	36.8	11.3	–
l_R (nm)	42 ± 33	14 ± 8	70
l_w (nm)	86 ± 52	101 ± 26	400
l_R/l_w (%)	49	14	17.5
R (nm)	22	91	286

by using the InterQuartile Range (IQR, fig. 4(e), inset), leading to $\xi_c \simeq 37\,\text{nm}$ for Canson® and $\xi_i \simeq 11\,\text{nm}$ for Inapa. Estimating the horizontal scale is more difficult to implement automatically. The asperities were thus picked manually. Table 1 reports their vertical (l_R) and horizontal (l_w) lengths, as well as their aspect ratio l_R/l_w and radius of curvature, $R \approx l_w^2/8l_R$. This estimation corroborates the IQR method, as $l_R \simeq \xi$.

5 Discussion and conclusion

At present, there does not exist any model explaining the link between the critical vibration velocity $(A\omega)_c$ and the geometrical characteristics of the asperities. Moreover, none of the lengths reported in table 1 makes a consensus as representative of the material frictional properties, although ξ and R are often used in contact models [5]. In a recent work, DeGiuli and Wyart [28] demonstrated that the energy of the external noise necessary to undergo the transition between stick-slip and continuous sliding is of order $(A\omega)_c^2$. Lastakowski *et al.* [21] proposed to compare this energy to the potential energy barrier to overcome the typical asperity height, ξ, leading to a dependence of the critical vibration velocity on the roughness height only, $(A\omega)_c \sim \sqrt{\xi}$. Here we find $\sqrt{\xi_c/\xi_i} \sim 1.8$, comparable to the critical velocity ratio of about 2 for Canson® and Inapa papers. Conversely, the ratio of about 2 between critical vibration velocities for Inapa paper and glass beads (granular friction) suggests a typical asperity scale for the grains $\xi_g = \xi_i/4 \simeq 3\,\text{nm}$. This value, however, is much smaller than estimates from AFM measurements previously made on sodosilicate glass beads [33]. In addition, note that the typical horizontal extent l_w and the radius of curvature R are the only lengths which vary monotonously with the critical vibration velocity for both granular and solid friction (table 1). If l_w alone can intuitively be discarded, the radius of curvature R appears as a good candidate to be the relevant lengthscale that controls the frictional properties —the smaller the radius of curvature is, the sharper are the asperities and the larger is the critical velocity of vibration to undergo the transition between stick-slip and continuous sliding.

Two additional points deserve to be discussed. First, in granular friction, the grains can move and, under given conditions, behave as an effective fluid. Recent experiments on dry granular media evidenced that controlled mechanical fluctuations, whose amplitude is much smaller than the granular assembly yield stress, are enough to provoke a macroscopic flow by a cumulative process: tiny effects integrated over time can lead to the system fluidization, as a secular drift mechanism [34,35]. However, although the global effective rheology depends also, in this case, on the product between the vibration amplitude and the frequency —in other words, on the vibration velocity, the authors do not find any critical velocity $(A\omega)_c$ as their system flows continuously for any, tiny, applied vibration. A possible explanation could be the existence of a smaller, microscopic, scale in the energy landscape basins, as recently suggested by Charbonneau *et al.* [36], which were not captured by the previous experimental devices but successfully captured by our experiments. It is striking, however, that solid friction also exhibits velocity weakening by external noise and a critical velocity, although there is neither grain mobility nor flow. Both in granular and solid friction, $(A\omega)_c$ is the threshold above which the yield stress vanishes and the system experiences a continuous motion.

Second, the aforementioned models and the asperities characterization (table 1) are based on the strong hypothesis that contacts are not altered by the slider. However, even for granular assemblies, even at low confinement pressure, a non-negligible fraction of contacts undergo a plastic deformation, leading to a dependence of the shear modulus on the height of the asperities only [33]. In the classical Greenwood-Williamson approach, plastic deformation of asperities starts when $\psi = (l_R/R)^{1/2}E/J > 1$, where E is the Young modulus and J the yield stress [5]. Taking $E \approx 20\,\text{GPa}$ and $J \approx 100\,\text{MPa}$ for paper [37] leads to $\psi \gg 1$ for both Canson® and Inapa. In our experimental conditions, a large fraction of contacts are therefore plastified, although the confinement pressure is low in our experiments. This suggests the existence of a "low" threshold $(A\omega)^*$ below which no frictional weakening occurs, as already mentionned for granular assemblies in numerical [38] and theoretical [28] studies, in agreement with laboratory fault-gouge experiments [12,39,8] and field measurements [40]. Both high-pressure experiments and field data suggest an increase of this threshold velocity with the normal load —of the order of 1 cm/s for 0.1 MPa and 10 cm/s for 10 MPa fault load [40]. This low threshold is not captured by our experimental device, the confinement pressure being probably too small for this effect to be significant. The difficulty in capturing both vibration velocity thresholds lies in the ability to measure tiny effects, while the normal load is considerably increased. The theoretical and experimental challenges are still open.

The authors thank Ludovic Bellon and Vincent Dolique for their help on SEM and AFM measurements. GV acknowledges financial support from PUCV DI Regular No. 039.438/2017. This work was supported by Programa de Cooperación Científica ECOS/CONICYT C14E07 and the Laboratoire International Associé "Matière: Structure et Dynamique" (LIA-MSD, France-Chile).

Author contribution statement

VV and J-CG conceived of the presented idea and the experimental setup. The experimental results were obtained for granular friction by HL, for paper-paper friction by CO under the supervision of GV. All authors discussed the results and contributed to the final manuscript mainly prepared by VV.

References

1. S. Sambursky, *The Physical World of Late Antiquity* (Princeton University Press, 1962) p. 188.
2. T. Baumberger, F. Heslot, B. Perrin, Nature **367**, 544 (1994).
3. C. Marone, Annu. Rev. Earth Planet. Sci. **26**, 643 (1998).
4. S. Nasuno, A. Kudrolli, A. Bak, J.P. Gollub, Phys. Rev. E **58**, 2161 (1998).
5. T. Baumberger, C. Caroli, Adv. Phys. **55**, 279 (2006).
6. G.S. Collins, H.J. Melosh, J. Geophys. Res. **108**, 2473 (2003).
7. A. Lucas, A. Mangeney, J.P. Ampuero, Nat. Commun. **5**, 3417 (2014).
8. K. Xia, S. Huang, C. Marone, Geochem. Geophys. Geosyst. **14**, 1012 (2013).
9. C. Levy, A. Mangeney, F. Bonilla, C. Hibert, E.S. Calder, P. Smith, J. Geophys. Res. **120**, 7536 (2015).
10. H.J. Melosh, J. Geophys. Res. **84**, 7513 (1979).
11. H.J. Melosh, Nature **379**, 601 (1996).
12. P.A. Johnson, X. Jia, Nature **437**, 871 (2005).
13. M.G. Rozman, M. Urbakh, J. Klafter, Phys. Rev. E **57**, 7340 (1998).
14. J. Gao, W.D. Luedtke, U. Landman, J. Phys. Chem. B **102**, 5033 (1998).
15. P.A. Johnson, H. Savage, M. Knuth, J. Gomberg, C. Marone, Nature **451**, 57 (2008).
16. R. Capozza, A. Vanossi, A. Vezzani, S. Zapperi, Phys. Rev. Lett. **103**, 085502 (2009).
17. R. Capozza, S.M. Rubinstein, I. Barel, M. Urbakh, J. Fineberg, Phys. Rev. Lett. **107**, 024301 (2011).
18. M.F. Melhus, I.S. Aranson, Granular Matter **14**, 151 (2012).
19. F. Giacco, E. Lippiello, M. Pica Ciamarra, Phys. Rev. E **86**, 016110 (2012).
20. F. Giacco, L. Saggese, L. de Arcangelis, E. Lippiello, M. Pica Ciamarra, Phys. Rev. Lett. **115**, 128001 (2015).
21. H. Lastakowski, J.C. Géminard, V. Vidal, Sci. Rep. **5**, 13455 (2015).
22. A. Gnoli, L. de Arcangelis, F. Giacco, E. Lippiello, M. Pica Ciamarra, A. Puglisi, A. Sarracino, Phys. Rev. Lett. **120**, 138001 (2018).
23. J.A. Dijksman, G.H. Wortel, L.T.H. van Dellen, O. Dauchot, M. van Hecke, Phys. Rev. Lett. **107**, 108303 (2011).
24. G. Wortel, O. Dauchot, M. van Hecke, Phys. Rev. Lett. **117**, 198002 (2016).
25. X. Jia, T. Brunet, J. Laurent, Phys. Rev. E **84**, 020301(R) (2011).
26. E. DeGiuli, G. Düring, M. Wyart, Phys. Rev. E **91**, 062206 (2015).
27. B. Ferdowsi, M. Griffa, R.A. Guyer, P.A. Johnson, C. Marone, J. Carmeliet, Geophys. Res. Lett. **42**, 9750 (2015).
28. E. DeGiuli, M. Wyart, Proc. Natl. Acad. Sci. U.S.A. **114**, 9284 (2017).
29. J.C. Gu, J.R. Rice, A.L. Ruina, S.T. Tse, J. Mech. Phys. Solids **32**, 167 (1984).
30. J.R. Rice, S.T. Tse, J. Geophys. Res. **91**, 521 (1986).
31. F.P. Bowden, D. Tabor, *The Friction and Lubrication of Solids I* (Clarendon Press, London, 1950).
32. M. Alava, K. Niskanen, Rep. Prog. Phys. **69**, 669 (2006).
33. H. Alarcón, J.C. Géminard, F. Melo, Phys. Rev. E **86**, 061303 (2012).
34. C. Derec, A. Ajdari, F. Lequeux, Eur. Phys. J. E **2**, 355 (2001).
35. A. Pons, A. Amon, T. Darnige, J. Crassous, E. Clément, Phys. Rev. E **92**, 020201(R) (2015).
36. P. Charbonneau, J. Kurchan, G. Parisi, P. Urbani, F. Zamponi, Nat. Commun. **5**, 3725 (2014).
37. S. Borodulina, A. Kulachenko, S. Galland, M. Nygårds, Nord. Pulp Paper Res. J. **27**, 318 (2012).
38. B. Ferdowsi, M. Griffa, R.A. Guyer, P.A. Johnson, J. Carmeliet, Acta Mech. **225**, 2227 (2014).
39. P.A. Johnson, B. Carpenter, M. Knuth, B.M. Kaproth, P.Y. Le Bas, E.G. Daub, C. Marone, J. Geophys. Res. **117**, B04310 (2012).
40. J. Gomberg, P.A. Reasenberg, P. Bodin, R.A. Harris, Nature **411**, 462 (2001).